JWMD Issue:5 2022
International Journal of Water Management and Diplomacy
e-ISSN:2717-8277

A Comparison of Image Classification on Synthetic Aperture Radar and Optical Images for Detection of Water Bodies: Case of Lake Burdur, Türkiye

Ben Forsyth 1*, Selin Guzel 2*

1,2, Middle East Technical University, Geodetic and Geographic Information Systems, Ankara, Türkiye

Correspondence Author, e-mail: Selin Güzel, e-mail: guzel.selin@metu.edu.tr

Abstract

This study presents a comparison of the classification results of two different datasets using two individual methods. This study utilizes both sentinel-1 data and Landsat data, with the first method involving the application of image classification on the sentinel data obtained and comparing the results. Additionally, data fusion as a second method was also performed on the sentinel VV polarisation and VH polarisation with Landsat 8 bands 3,5 and 8 in an attempt to improve the accuracy results of the classification. The classification results of the first method and the second method are compared in this paper. Water detection was the primary goal of this study, leading to these specific choices of Landsat bands.

Keywords: Water body detection; image classification; synthetic aperture Radar; optical imagery; image fusion

1. INTRODUCTION

The majority of Earth's surface is covered with water and it is an important subject to the interest of people (Wang et al., 2011) as productive and ecologically diverse ecosystems are located along these water bodies, however, the extent of these bodies is getting smaller each year at alarming rates (Huang et al., 2018). Accurate assessment and analyses of the spatial extent of water bodies over time play a crucial role in monitoring the effects of climate change and show how this phenomenon is affecting the environment, ecology as well as water resources. Applications of Remote Sensing are widely used for these analyses since they provide advantages such as broad observation areas, short time periods of observation and easy acquisition of necessary information from areas of interest (Fu et al., 2007).

SAR systems have shown their abilities for countless Earth observation applications (Krieger et al., 2010) since they provide high-resolution and two-dimensional images which are not dependent on daylight, cloud coverage and various weather conditions (Moreira et al., 2013). In addition to these, they are very sensitive to open water so they are utilised for water surface detection (Huang et al., 2018). Despite all these advantages, SAR data has limited availability (Santoro et al., 2015) and this causes discontinuities in spatial and temporal data. Moreover, analysis of SAR data can be

e-ISSN:2717-8277

complicated which can lead to misinterpretation. complications of using SAR data, improving classification accuracy (L. et al., 2009).

Fusion of different sensors which can detect different aspects of water bodies and their surroundings, can be a solution to overcome the This paper focuses on comparing the classification outputs provided by the multiple data sources, the sources used were Sentinel-1 and Landsat-8 data. Data fusion methods were used on these data to improve classification results.

2. STUDY AREA

The area chosen for this study is Lake Burdur which is among the largest and deepest lakes in Turkey and is located at the southwest. It is a tectonic and a closed basin lake located between Burdur and Isparta provinces and it has 250 km^2 of water surface. As well as its distinguished size, it has great ecological importance since it is a habitat for globally threatened bird species (RAMSAR).

Figure 1. Location of the Study Area (www.earth.google.com)

1. DATASET

For extracting the water extent of Lake Burdur, two Sentinel-1A and one Landsat-8 data from November 2022 were used. C band Sentinel-1 Ground Range Detected (GRDH), Interferometric Wide (IW), dual polarimetry (VV and VH mode data were acquired with) descending pass direction. In addition to the SAR data, the three bands that present the water surface the best of all the Landsat bands were green, red and panchromatic.

JWMD Issue:5 2022
International Journal of Water Management and Diplomacy
e-ISSN:2717-8277

Table 1. Characteristics of Sentinel-1 and Landsat-8 Data

Sentinel-1	**Acquisition Date**	**Polarization**	**Pass Direction**	**Mode**
	20.11.2022	VV-VH	Descending	IW GRDH
Landsat-8	**Acquisition Date**	**Spectral Resolution**	**Spatial Resolution**	**Temporal Resolution**
	14.11.2022	Multispectral: 0.43-0.67 μm	15 m (Panchromatic)	16 days
		IR: 0.85-2.29 μm	30 m (Multispectral)	
		Pan: 0.50 – 0.68 μm	100 m (Thermal IR)	
		Circus: 1.36 – 1.38 μm		

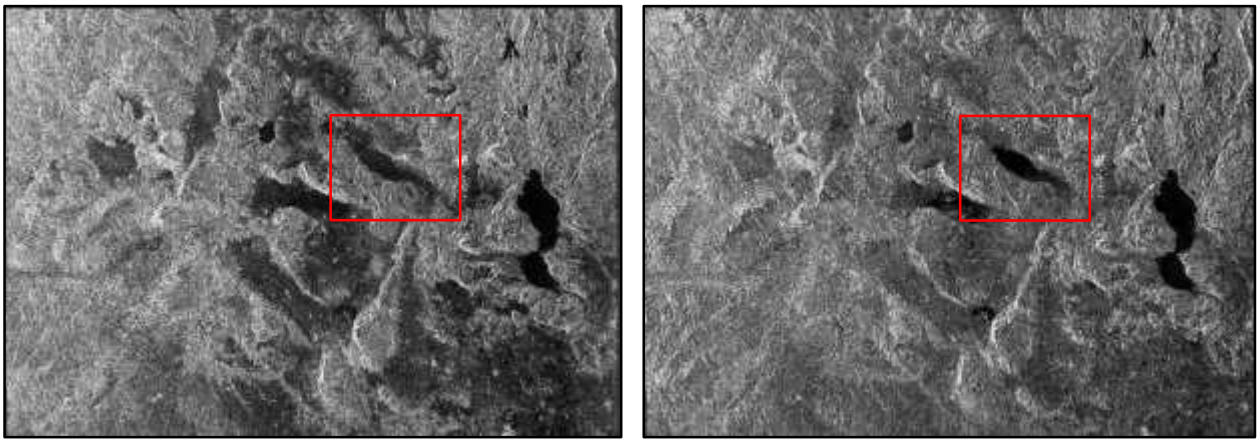

(a) (b)

Figure 2. Sentinel-1 scene acquired on 20 November 2022, VH polarization (a), VV polarization (b) and the location of the study area

Issue:5 2022
International Journal of Water Management and Diplomacy
e-ISSN:2717-8277

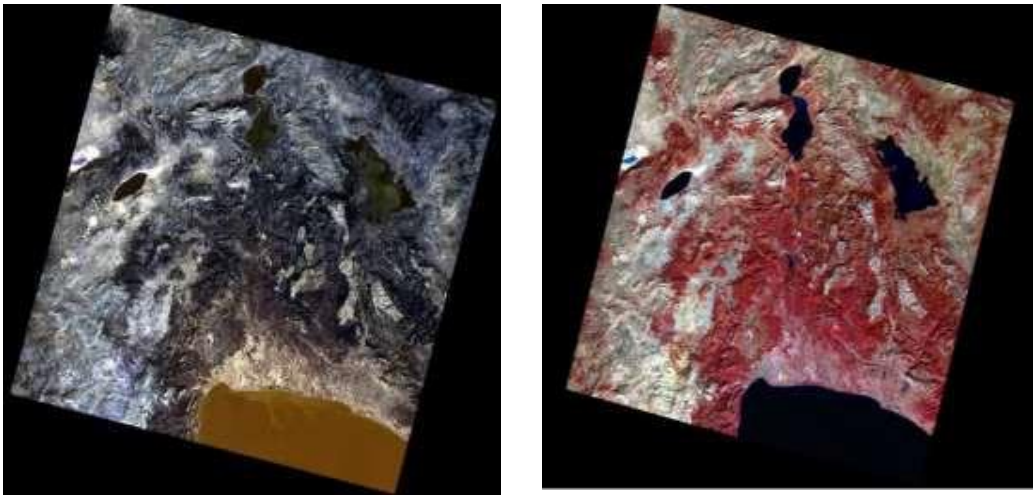

(a) (b)

Figure 3. Concatenated Landsat-8 image with bands 3, 5, 8 (Green, NIR, Panchromatic) (a), false colour image (NIR, Red, Green) (b)

2. MATERIALS AND METHODS

The workflow of the process chain, as can be seen in Figure 4, is composed of the following steps; pre- processing of sentinel images, landsat-8 and sentinel-1 data fusion, classification of sentinel-1 and fused data using random forest classifier and accuracy assessment of the results. To be able to perform the mentioned steps Sentinel Application Platform (SNAP), QGIS and Monteverdi software were used.

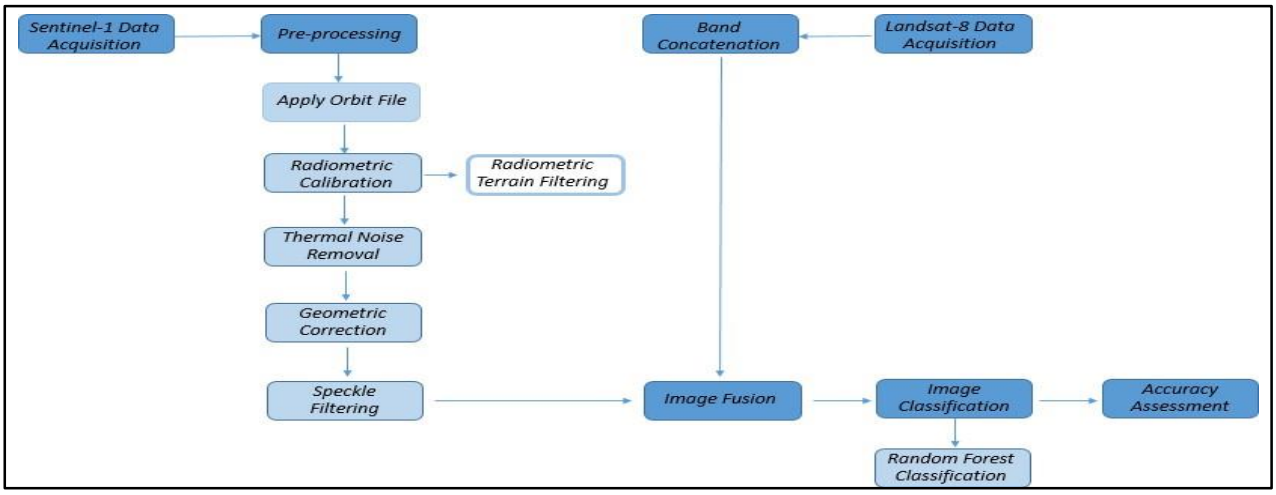

Figure 4. Workflow of the Process Chain

e-ISSN:2717-8277

2.1. Pre-processing of the Data

Pre-processing of the Sentinel-1 data was conducted on SNAP software for each VV and VH modes and the process was initialised by using Apply Orbit File (AOF) to improve geocoding results. Radiometric calibration was applied next to correct the signal intensity. Radiometric Terrain Flattening was performed then to remove the topographic effect from the study area. Next, thermal noise needed to be removed and the Thermal Noise Removal command was used for this purpose. After applying radiometric corrections, geometric correction of the image needed to be conducted. This was performed by Range- Doppler Terrain Correction and images were projected into the Universal Transverse Mercator (UTM) or World Geodetic System 1984 (WGS84) together with the corrections of distortion effects such as shadow or layover, which occurred during the acquisition. Radar images produced some noise called speckle and to enhance the quality of the data speckle filtering operation was needed to be used. Before filtering the image, the study area was clipped to reduce the required processing time of filtering, and then by using Lee Filter 7x7, the effects of speckles were reduced.

For the Landsat image, the three bands that present the water surface the best of all the Landsat-8 bands which were green, red and panchromatic were concatenated using Monteverdi software, then it was clipped using the same coordinates as the corners for each image.

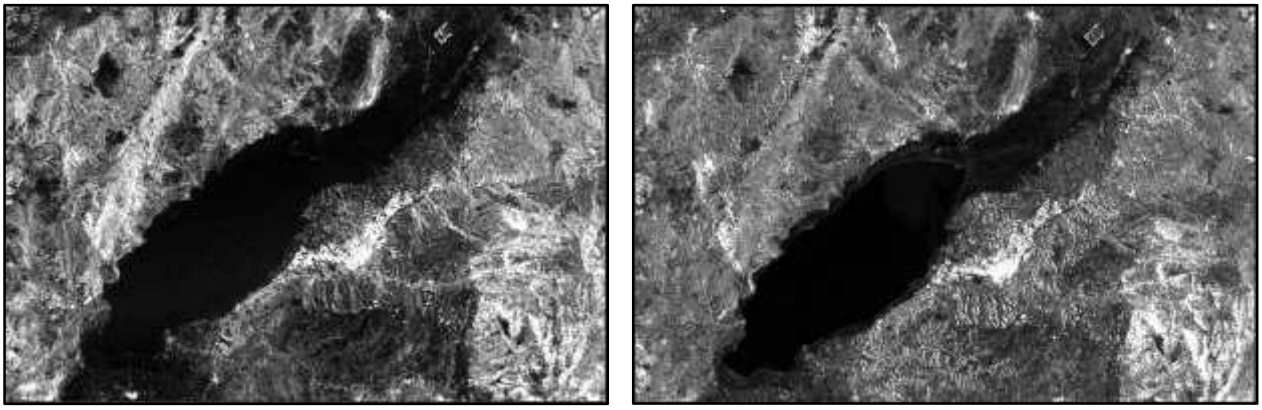

(a) (b)

Figure 5. Post-processed Sentinel-1 image, VH polarization (a), VV polarization (b)

JWMD Issue:5 2022
International Journal of Water Management and Diplomacy
e-ISSN:2717-8277

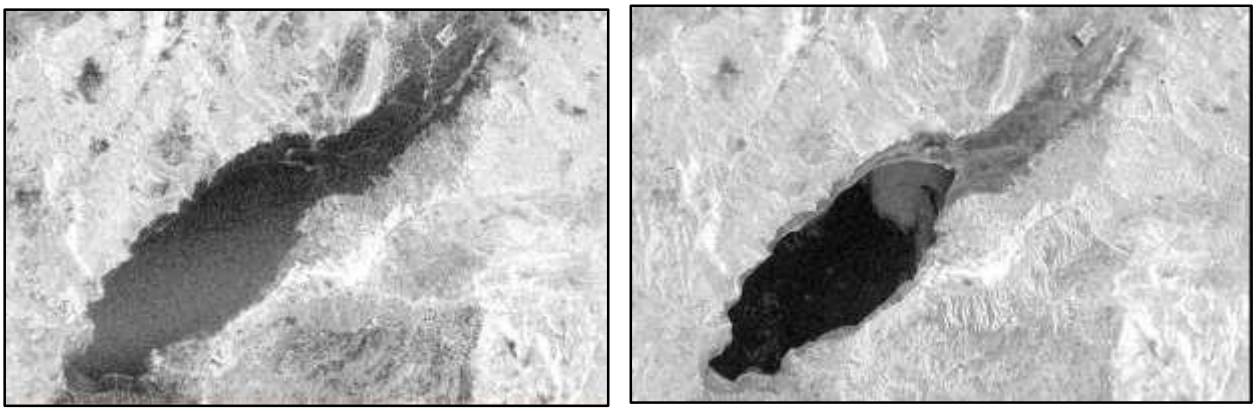

(a) (b)

Figure 6. Post-processing images of SAR data converted from linear (sigma values) to decibels, VH polarization (a), VV polarization (b)

(a) (b)

Figure 7. Clipped Landsat-8 image with bands 3, 5, 8 (Green, NIR, Panchromatic) (a), false colour image (NIR, Red, Green) (b)

2.2. Image Fusion

Image fusion is a technique used to combine the geometric detail of a panchromatic image having a high spatial resolution and the colour information of a multispectral image having a low spatial resolution to create a high-resolution multispectral image (Quang et al., 2019). For this study, a fusion of the images was created using sentinel-1 as high resolution and Landsat image as coloured data so that a high-resolution multispectral image would be obtained. The image concatenation tool from the Monteverdi application was used as the method for this. Bands 3,5 and 8 were taken from the Landsat image and concatenated with the sentinel VV image, and then again with the sentinel VH image. Bands 3 (green) and 5 (NIR) were chosen for the Landsat image as these bands differentiate water more clearly from other objects. Furthermore, Band 8 (panchromatic) was chosen to add extra special details such as the extent of the water.

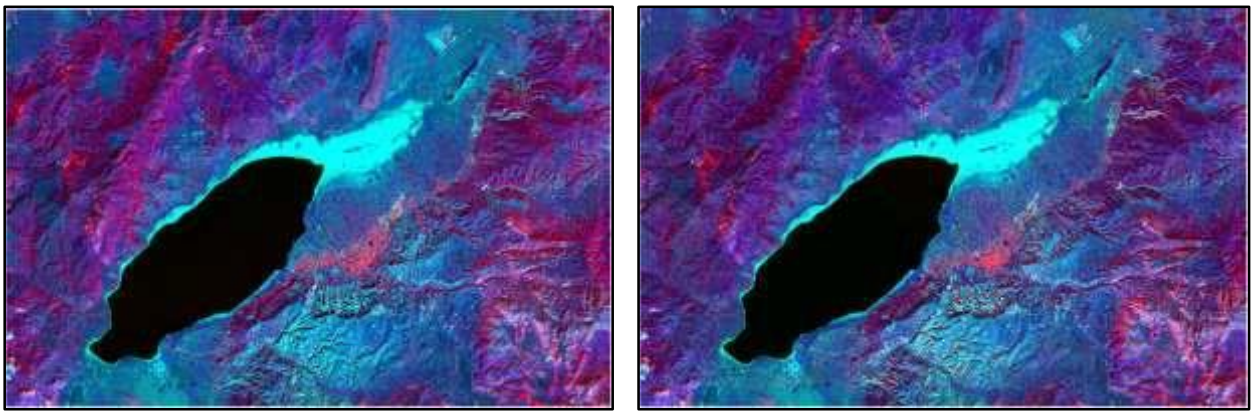

(a) (b)

Figure 8. Landsat-8 bands 3,5 and 8 fused with VH sentinel data (a), Landsat-8 bands 3,5 and 8 fused with VV sentinel data (b)

Fusing these Landsat and sentinel (VV, VH) data sets created two separate high-resolution images suitable for classification.

2.3. Image Classification

Random forest classification has proven to be a reliable and effective alternative to other regular pixel-based classifications and is specifically useful for classifying satellite imagery. It is seen as one of the most successful classification methods in the community (Bayik et al., 2018). The classification was carried out on the sentinel VV data and the sentinel VH data separately, as well as the sentinel VV fused with the Landsat data and the sentinel VH fused with the Landsat data. The semi-automatic classification plugin (SCP) in QGIS was used to perform the classification.

Training classes were created as polygons covering the required areas, only two main classes were created, these being 'water' and 'other'. The 'Other' class had multiple different subclasses which

e-ISSN:2717-8277

were created to help define the main class more accurately and hopefully cancel out any misclassification of water.

2.4. Accuracy Assessment

Once again, the SCP extension in QGIS was used for calculating the accuracies of the classifications. A separate validation layer using the same classes was created. This layer covered separate areas to the classification training data and, since there was no access to ground truth data, each polygon in the validation set was assigned to a class based on looking at the image. The accuracy assessment tool was used with the validation layer being used on the classification raster. This process was carried out on each classification output, with the same validation layer was used for each one.

3. RESULTS AND CONCLUSIONS

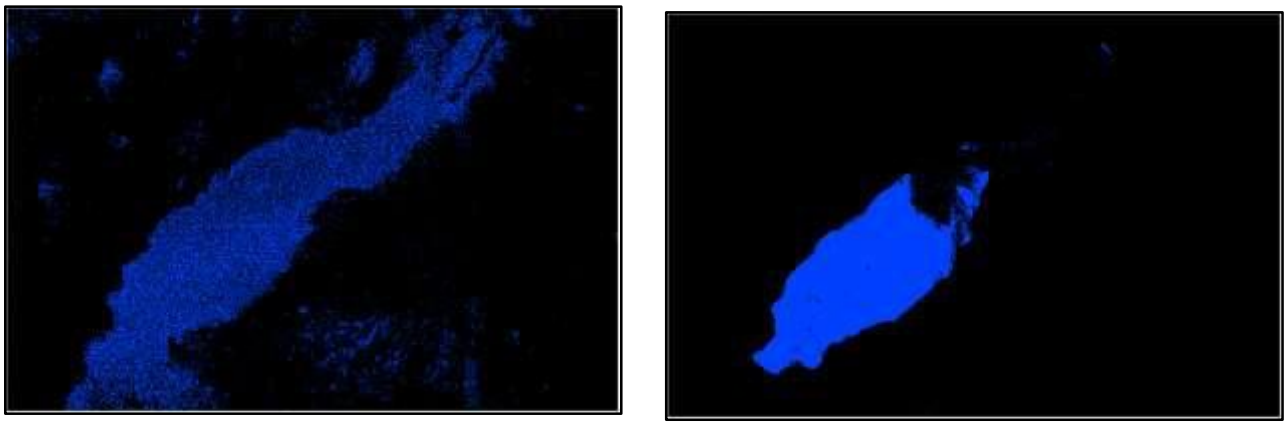

(a) (b)

Figure 9. RFC classification of sentinel VH data with water as blue and non-water as black (a), RFC classification of sentinel VV data with water as blue and non-water as black (b)

From visual inspection, it can be seen that the classification of VH data performed poorly compared to that of the VV data, with the VH classification causing misclassifying lots of non-water areas as water.

Issue:5 2022
International Journal of Water Management and Diplomacy
e-ISSN:2717-8277

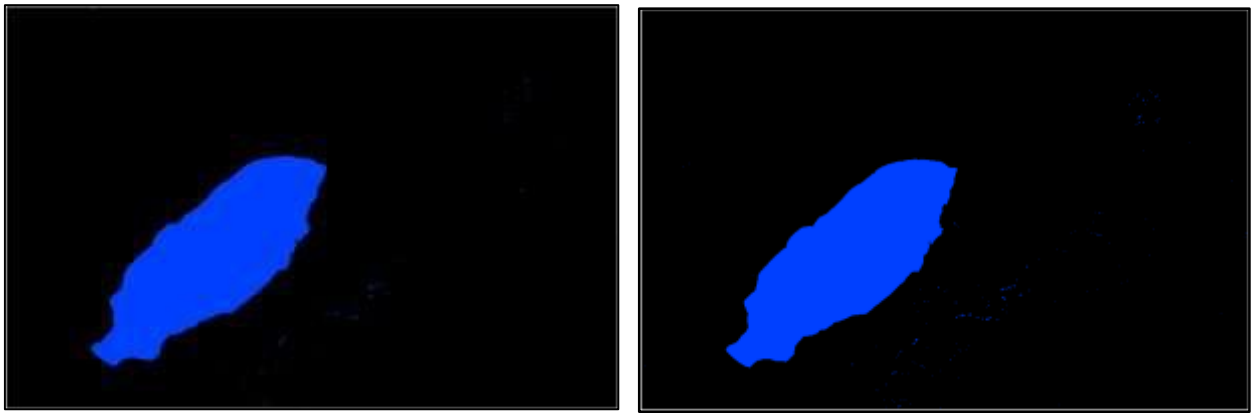

(a) (b)

Figure 10. RFC classification of fused sentinel VH with Landsat data with water as blue and non-water as black (a), RFC classification of fused sentinel VV with Landsat data with water as blue and non-water as black (b)

From visual inspection, it can be seen that both VH and VV sentinel data fused with Landsat data provides a very accurate water extent with minimal misclassification.

From visual inspection of the Random Forest classifier outputs, it was observed that the classifications made on both sentinel-1 data sets did not show the correct water extent. The classification was performed slightly better when VV mode was used as the input raster, compared to VH mode. When fused data was classified, however, very accurate visual results were observed. These findings were further supported by the histograms showing the decibel backscatter values for both VV and VH polarisations.

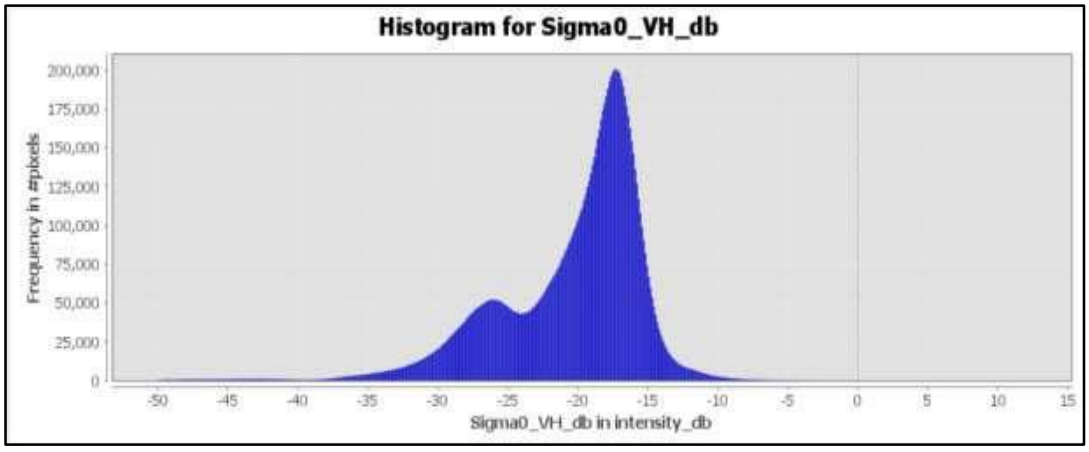

Figure 11. Histogram showing the backscatter values of the VH SAR image.

JWMD Issue:5 2022
International Journal of Water Management and Diplomacy
e-ISSN:2717-8277

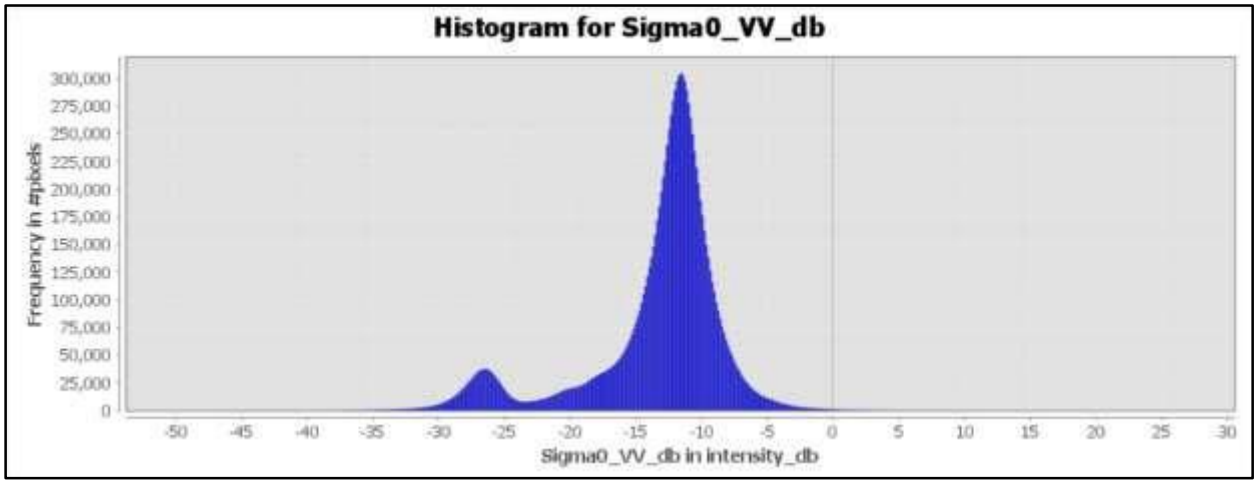

Figure 12. Histogram showing the backscatter values of the VV SAR image.

In both histograms, there are two peaks present with each peak representing different surface types according to their backscatter value. The smaller peak represents water with the larger peak representing other land covers such as vegetation, bare land, urban, etc. Water pixels are normally supposed to have a backscatter value of roughly -24 db. After examining the individual pixel values of the image, for this case water values were found to be between -32 db and -24 db for the VV polarisation and -24 db and -36 db for VH polarisation.

Table 2. Accuracy table for classification of Sentinel VH image

Sentinel_VH	Water	Other	Total
Water	273990	94630	368620
Other	242430	1779675	2022105
Total	516420	1874305	2390725
Producers Accuracy [%]	44.1047	96.4205	
Users Accuracy [%]	74.3286	88.011	
Overall Accuracy [%]	86.4662		
Kappa	0.4799		

The table above shows the classification accuracy results of the VH sentinel nonfused image. Producers' accuracy for the 'water' class is 44% whereas users' accuracy for water was 74%. The overall accuracy was calculated as 86% with a low kappa coefficient value of 0.48.

Table 3. Accuracy table for classification of Sentinel VV image

Sentinel_VV	Water	Other	Total
Water	393776	4051	397827
Other	122644	1870254	1992898
Total	516420	1874305	2390725
Producers Accuracy [%]	60.4152	99.8971	
Users Accuracy [%]	98.9817	93.8459	
Overall Accuracy [%]	94.291		
Kappa	0.7202		

The table above shows the classification accuracy results of the VV sentinel nonfused image. Producers' accuracy for the 'water' class is 60% whereas users' accuracy for water was 99%. The overall accuracy was calculated as 94% with a moderate kappa coefficient value of 0.72.

Classification using VV data gave better overall accuracy than that of the VH data, with the overall accuracy for the VV classification being 7.8448% higher than that of the VH classification. VV also produced higher users and producers' accuracy, as well as having a higher kappa coefficient. Notably, the producer's accuracy for water seems to be relatively low across both polarisations, which has led to a lower kappa coefficient across both classifications, especially the VH image. Despite this, users' accuracy remained relatively accurate for both data sets. Furthermore, the results line up with the visual representation of the classification, wherein the classification of VH data misclassified large portions of the area.

Table 4. Accuracy table for classification of Sentinel VH image fused with Landsat bands 3,5 and 8

Sentinel_VH/Landsat	Water	Other	Total
Water	516420	1259	517679
Other	0	1873046	1873046
Total	516420	1874305	2390725
Producers Accuracy [%]	100	99.9744	
Users Accuracy [%]	99.7568	100	
Overall Accuracy [%]	99.9769		
Kappa	0.9987		

The table above shows the classification accuracy results of the VH sentinel image fused with Landsat data. Producers' accuracy for the 'water' class is 100% whereas users' accuracy for water was 99.7568%. The overall accuracy was calculated as 99.9769% with a high kappa coefficient value of 0.9987.

Table 5. Accuracy table for classification of Sentinel VV image fused with Landsat bands 3,5 and 8

Sentinel_VV/Landsat	Water	Other	Total
Water	516420	1151	517571
Other	0	1873154	1873154
Total	516420	1874305	2390725
Producers Accuracy [%]	100	99.9753	
Users Accuracy [%]	99.7776	100	
Overall Accuracy [%]	99.9778		
Kappa	0.9988		

The table above shows the classification accuracy results of the VV sentinel image fused with Landsat data. Producers' accuracy for the 'water' class is 100% whereas users' accuracy for water was 99.7776%. The overall accuracy was calculated as 99.9778% with a high kappa coefficient value of 0.9988.

Classification of the fused images showed much closer overall accuracy results as well as much closer producers' and users' accuracies across the classes, leading to high kappa coefficients. Overall accuracies were over 99%, showing very high levels of classification across both VV and VH data, nevertheless, the fused VV data showed a very slightly higher accuracy result than that of the VH data.

The fused images in conjunction with the random forest classifier produced the highest accuracy results, specifically the fused images using the sentinel VV data.

The most accurate results of all classification outputs were shown to be the fused sentinel and Landsat images in conjunction with the RFC. The sentinel images by themselves did not show very accurate results and caused misclassification of land areas as water. This could be due to the fact that the images were obtained in November which is a rainy season in Lake Burdur, causing the moisture in land areas to be detected by the SAR sensors. This however was not a problem for Landsat data. That is why sentinel images

showed relatively poor accuracy results compared to the fused images. To improve the use of using sentinel data exclusively in potential future research, time series data can be used to improve the classification results of SAR data. This can be useful in situations that Landsat data cannot be acquired, for example, bad weather conditions.

While VH is more effective at detecting rough surfaces due to the depolarisation effect of volume scattering (Amazirh et al., 2018), VV is much more efficient at differentiating water from surrounding surfaces and vegetation (Twele et al., 2016). This can be seen just from the visuals of the SAR images. The VV image shows that Burdur Lake stands out and is much more defined in contrast with the surrounding areas, whereas in the VH image, some areas surrounding the lake are much less defined and look similar to the water.

In the VH non-fused image, some areas are much less defined and look similar to the water, they look as if they have low backscatter values similar to the water surfaces. This is backed up by the low overall accuracy of the VH image classification. Furthermore, VH polarised data could have led to a very low land-water contrast, resulting in a higher amount of misclassifications. Not only were some areas misclassified as water, but some for the actual water surface, wrong results were still being produced. This can be seen as parts of the lake are classified as 'other', rather than 'water'. The VH data also caused misclassification in a large portion of agricultural farmland southwest of the lake, due to the low polarisation and low backscatter value in VH polarisation (Twele et al., 2016). VH polarisation created water-lookalike areas due to these effects.

This can be seen with the backscatter values for the VH polarisation not differentiating water from land as well as the VV. This can be seen in Figure 11 with the histogram showing the backscatter values for VH polarisation. It is observed that there is a much smoother transition between both peaks in the VH histogram meaning that water and other land covers are less distinguished from each other. The opposite can be seen in Figure 12 which shows the VV backscatter values histogram, as can be seen there, there is a much sharper curve between the two peaks, signifying that there is more differentiation between water and other land surfaces.

As can be seen in the classification of the non-fused VV image, there was an area of water that was misclassified as other in the northeast portion of the lake. This is due to the slightly higher backscatter values of the water in this area, with most pixels having a rough value of -18 which is a value associated with forests, paths, roads, etc. This area can be seen as brighter in Figure 6 showing the SAR images backscatter decibel values. This could be due to this area being shallower in water depth than other areas of the lake since C band VV and VH polarisation have been shown to be sensitive to water depth (Zhang et al., 2022).

Overall, VV sentinel data fused with Landsat bands 3,5, and 8 showed the highest accuracy results as expected. This is mainly due to the fact that, as previously discussed, VV data is much better at differentiating water from surrounding areas when compared to VH data. In addition, the Landsat bands chosen were specifically chosen as they extract water from images with the highest

effectiveness leading to higher accuracy of the fused images instead of just the sentinel images by themselves.

SAR data by itself is very useful for gathering data in certain conditions and is a powerful tool in identifying land cover, however, it still has its flaws and classification on a single polarisation by itself will not lead to accurate results. The SAR data in combination with optical images has shown a much higher accuracy in classification once fused together. This study in particular focused on water and thus selected the polarisations and bands that were most suitable for the extraction of water surfaces, but this principle of fusing can still be applied to other classification problems using other bands in order to increase classification accuracy.

4. REFERENCES

A. Moreira, P. Prats-Iraola, M. Younis, G. Krieger, I. Hajnsek and K. P. Papathanassiou, "A tutorial on synthetic aperture radar," in IEEE Geoscience and Remote Sensing Magazine, vol. 1, no. 1, pp. 6-43, March 2013, doi: 10.1109/MGRS.2013.2248301.

Amazirh, A., Merlin, O., Er-Raki, S., Gao, Q., Rivalland, V., Malbeteau, Y., Khabba, S., & Escorihuela, M. J. (2018). Retrieving surface soil moisture at high spatio-temporal resolution from a synergy between sentinel-1 radar and Landsat Thermal Data: A study case over bare soil. Remote Sensing of Environment, 211, 321–337. https://doi.org/10.1016/j.rse.2018.04.013

Bayik, C., Abdikan, S., Ozbulak, G., Alasag, T., Aydemir, S., & Balik Sanli, F. (2018). Exploiting multi-temporal sentinel-1 SAR data for flood extent mapping. *The International Archives of the Photogrammetry, Remote Sensing and Spatial Information Sciences*, *XLII-3/W4*, 109–113. https://doi.org/10.5194/isprs- archives-xlii-3-w4-109-2018

Fu, J., Wang, J., & Li, J. (2007). Study on the automatic extraction of water body from TM image using decision tree algorithm. *SPIE Proceedings*. https://doi.org/10.1117/12.790602

Huang, W.; DeVries, B.; Huang, C.; Lang, M.W.; Jones, J.W.; Creed, I.F.; Carroll, M.L. Automated Extraction of Surface Water Extent from Sentinel-1 Data. *Remote Sens.* **2018**, *10*, 797. https://doi.org/10.3390/rs10050797

Krieger, G., Hajnsek, I., Papathanassiou, K. P., Younis, M., & Moreira, A. (2010). Interferometric synthetic aperture radar (SAR) missions employing formation flying. *Proceedings of the IEEE*, *98*(5), 816–843. https://doi.org/10.1109/jproc.2009.2038948

L., L., Riordan, K., B., R., Miller, N., & Nowels, M. (2009). Improving wetland characterization with multi-sensor, multi-temporal SAR and optical/infrared data fusion. *Advances in Geoscience and Remote Sensing*. https://doi.org/10.5772/8327

Quang, N. H., Tuan, V. A., Hao, N. T., Hang, L. T., Hung, N. M., Anh, V. L., Phuong, L. T., & Carrie, R. (2019). Synthetic aperture radar and optical remote sensing image fusion for flood monitoring in the Vietnam Lower Mekong basin: A prototype application for the Vietnam Open Data Cube. *European Journal of Remote Sensing*, *52*(1), 599–612. https://doi.org/10.1080/22797254.2019.1698319

Ramsar Sites Information Service. Lake Burdur | Ramsar Sites Information Service. (n.d.). Retrieved December

30, 2022, from https://rsis.ramsar.org/ris/658

Santoro, M., Wegmüller, U., Lamarche, C., Bontemps, S., Defourny, P., & Arino, O. (2015). Strengths and weaknesses of multi-year Envisat Asar Backscatter measurements to map permanent open water bodies at global scale. Remote Sensing of Environment, 171, 185–201. https://doi.org/10.1016/j.rse.2015.10.031
Twele, A., Cao, W., Plank, S., Martinis, S., 2016. Sentinel-1-based flood mapping: a fully automated processing chain. International Journal of Remote Sensing 37, 2990–3004

Wang, Y., Ruan, R., She, Y., & Yan, M. (2011). Extraction of water information based on Radarsat Sar and Landsat ETM+. Procedia Environmental Sciences, 10, 2301–2306. https://doi.org/10.1016/j.proenv.2011.09.359
Zhang, B., Wdowinski, S., Gann, D., Hong, S.H. and Sah, J., 2022. Spatiotemporal variations of wetland backscatter: The role of water depth and vegetation characteristics in Sentinel-1 dual-polarization SAR observations. Remote Sensing of Environment, 270, p.11

Received: December 10 2023
Accepted : January 07 2024